Aberrant expression and subcellular localization of ECT2 drives colorectal cancer progression and growth

Danielle R. Cook[1], **Melissa Kang**[2], **Timothy D. Martin**[3], **Joseph A. Galanko**[2], **Gabriela H. Loeza**[4], **Dimitri G. Trembath**[5,6], **Verline Justilien**[7], **Karen A. Pickering**[8], **David F. Vincent**[8], **Armin Jarosch**[9], **Philipp Jurmeister**[9], **Andrew M. Waters**[5], **Priya S. Hibshman**[5,10], **Andrew D. Campbell**[8], **Catriona A. Ford**[8], **Temitope O. Keku**[2], **Jen Jen Yeh**[3,5,11], **Michael S. Lee**[4,5], **Adrienne D. Cox**[3,5,12], **Alan P. Fields**[7], **Robert S. Sandler**[2], **Owen J. Sansom**[8,13], **Christine Sers**[9,14,15], **Antje Schaefer**[3,5,#], **Channing J. Der**[1,3,5,9,#]

[1]Division of Chemical Biology and Medicinal Chemistry, University of North Carolina at Chapel Hill, Chapel Hill, North Carolina.

[2]Center for Gastrointestinal Biology and Disease, University of North Carolina at Chapel Hill, Chapel Hill, North Carolina.

[3]Department of Pharmacology, University of North Carolina at Chapel Hill, Chapel Hill, North Carolina.

[4]Department of Medicine, University of North Carolina at Chapel Hill, Chapel Hill, North Carolina.

[5]Lineberger Comprehensive Cancer Center, University of North Carolina at Chapel Hill, Chapel Hill, North Carolina.

[6]Department of Pathology and Laboratory Medicine, University of North Carolina at Chapel Hill, Chapel Hill, North Carolina.

[7]Department of Cancer Biology, Mayo Clinic Comprehensive Cancer Center, Jacksonville, Florida.

[8]Cancer Research UK Beatson Institute, United Kingdom.

[9]Charité Universitätsmedizin Berlin, Institute of Pathology, Laboratory of Molecular Tumor Pathology and Systems Biology, Berlin, Germany.

[#]**Co-corresponding Authors:** Channing J. Der, University of North Carolina at Chapel Hill, Lineberger Comprehensive Cancer Center, 450 West Drive, Chapel Hill, NC 27599, USA, Phone: 919-966-5634; cjder@med.unc.edu; Antje Schaefer, University of North Carolina at Chapel Hill, Lineberger Comprehensive Cancer Center, 450 West Drive, Chapel Hill, NC 27599, USA, Phone: 919-962-1057; antje_schaefer@med.unc.edu.

Authors' Contribution

Conception and design: D.R. Cook, T.O. Keku, J.J. Yeh, C.J. Der

Development of methodology: D.R. Cook, T.O. Keku, J.J. Yeh, C.J. Der

Acquisition of data (provided animals, acquired and managed patients, provided facilities, etc.): D.R. Cook, M. Kang, T.D. Martin, M.S. Lee, A.M. Waters, P.S. Hibshman, G.H. Loeza, R.S. Sandler, D.G. Trembath, K. Pickering, V. Justilien, D. Vincent, A. Jarosch, P. Jurmeister, A.D. Campbell, C. A. Ford, A. Schaefer

Analysis and interpretation of data (e.g., statistical analysis, biostatistics, computational analysis): D.R. Cook, A.D. Campbell, C. A. Ford, T.O. Keku, J.J. Yeh, A.P. Fields, O. Sansom, A.D. Cox, C. Sers, A. Schaefer, C.J. Der

Writing, review and/or revision of the manuscript: D.R. Cook, V. Justilien, A.D. Campbell, T.O. Keku, J.J. Yeh, M.S. Lee, A.P. Fields, A.D. Cox, O. Sansom, C. Sers, A. Schaefer, C.J. Der

Administrative, technical, or material support (i.e., reporting or organizing data, constructing databases): T. Keku, J.J. Yeh, A.D. Cox, A.P. Fields, R. Sandler, O. Sansom, C. Sers, A. Schaefer

Study supervision: T.O. Keku, J.J. Yeh, O. Sansom, C. Sers, C.J. Der

Author Manuscript

[10]Departments of Cell Biology and Physiology, University of North Carolina at Chapel Hill, Chapel Hill, North Carolina.

[11]Department of Surgery, University of North Carolina at Chapel Hill, Chapel Hill, North Carolina.

[12]Department of Radiation Oncology, University of North Carolina at Chapel Hill, Chapel Hill, North Carolina.

[13]Institute of Cancer Sciences, University of Glasgow, United Kingdom.

[14]German Cancer Consortium (DKTK), German Cancer Research Center (DKFZ), Heidelberg, Germany.

[15]Berlin Institute of Health (BIH), Berlin, Germany

Abstract

ECT2 is an activator of RHO GTPases that is essential for cytokinesis. Additionally, ECT2 was identified as an oncoprotein when expressed ectopically in NIH/3T3 fibroblasts. However, oncogenic activation of ECT2 resulted from N-terminal truncation, and such truncated ECT2 proteins have not been found in cancer patients. In this study, we observed elevated expression of full-length ECT2 protein in preneoplastic colon adenomas, driven by increased *ECT2* mRNA abundance and associated with *APC* tumor suppressor loss. Elevated ECT2 levels were detected in the cytoplasm and nucleus of colorectal cancer (CRC) tissue, suggesting cytoplasmic mislocalization as one mechanism of early oncogenic ECT2 activation. Importantly, elevated nuclear ECT2 correlated with poorly differentiated tumors, and a low cytoplasmic:nuclear ratio of ECT2 protein correlated with poor patient survival, suggesting that nuclear and cytoplasmic ECT2 play distinct roles in CRC. Depletion of ECT2 reduced anchorage-independent cancer cell growth and invasion independent of its function in cytokinesis, and loss of *Ect2* extended survival in a *Kras*^{G12D} *Apc*-null colon cancer mouse model. Expression of ECT2 variants with impaired nuclear localization or guanine nucleotide exchange catalytic activity failed to restore cancer cell growth or invasion, indicating that active, nuclear ECT2 is required to support tumor progression. Nuclear ECT2 promoted ribosomal DNA transcription and ribosome biogenesis in CRC. These results support a driver role for both cytoplasmic and nuclear ECT2 overexpression in CRC and emphasize the critical role of precise subcellular localization in dictating ECT2 function in neoplastic cells.

Keywords

Colorectal cancer; cytokinesis; ECT2; guanine nucleotide exchange factor; RHO GTPase

Introduction

RAS homologous RHO small GTPases (e.g., RHOA, RAC1) function as key signaling nodes that are activated by extracellular stimuli acting on a variety of cell surface receptors (1). RHO GTPases regulate a diverse spectrum of signaling networks that control actin organization, cell cycle and gene expression. Therefore, it is not unexpected that the aberrant activity of RHO GTPases has been implicated in cancer (2–4). Whereas RAS GTPases

are mutated frequently in a diversity of cancer types (2,5,6), only recently has mutational activation of RHOA and RAC1 been identified, associated with a limited spectrum of cancer types (2,4,7–9). *RHOA* mutations are found predominantly in diffuse gastric carcinomas and peripheral T-cell lymphomas, whereas *RAC1* mutations are found near exclusively in cutaneous melanomas.

More commonly, RHO GTPase function is disrupted in cancers by indirect mechanisms (7,10,11). Like RAS, RHO GTPases are highly regulated GTP-GDP-driven binary on-off switches that relay extracellular signals to cytoplasmic signaling networks (2,10,12). In response to activated receptors, RHO-selective guanine nucleotide exchange factors (RHOGEFs) accelerate the intrinsic GDP-GTP exchange activity and stimulate formation of active GTP-bound RHO. Active RHO-GTP binds multiple effectors, inducing downstream signaling. The activated state is transient, with RHO-selective GTPase activating proteins (RHOGAPs) catalyzing the RHO intrinsic GTPase activity, returning RHO to the inactive GDP-bound state. Aberrant activation of RHOGEFs and loss-of-function of RHOGAPs are found in cancer, leading to persistent formation of active RHO-GTP and stimulus-independent activation of effector signaling (7,10).

Dbl family RHOGEFs were discovered initially as oncogenes and provided the first evidence that aberrant RHO activation may drive cancer (10). The RHOGEFs DBL, ECT2 and VAV were detected in the same type of NIH/3T3 mouse fibroblast focus formation assays (13–15) that identified mutationally activated *RAS* genes in cancer (16). Their mechanisms of activation involved amino-terminal deletion of sequences upstream of the RHOGEF catalytic Dbl homology (DH) domain. An amino-terminally truncated ECT2 (N-ECT2) resulted in the loss of the nuclear localization sequences (NLS) (14), suggesting that mislocalization of the normally nuclear restricted ECT2 to the cytoplasm contributed to its transforming activity. Disruption of the NLS motifs alone in full-length ECT2 created a transforming protein when expressed in NIH/3T3 cells, suggesting that ECT2 oncogenic function can be activated simply by mislocalization from the nucleus to the cytoplasm (17).

Despite the frequent detection of amino-terminally truncated, oncogenic RHOGEFs in multiple independent studies, these activation events occurred as a consequence of *in vitro* DNA manipulation rather than bona fide genetic events in cancer cells (10). Surprisingly, despite their potent transforming activities in NIH/3T3 cells, truncated RHOGEFs have not been found in human cancers (10,11). Subsequent studies demonstrated that ECT2 oncogenic function is more complex than simple mislocalization from the nucleus to the cytoplasm. Evaluation of ECT2 overexpression in lung cancer found distinct ECT2 functions in the cytoplasm and nucleus, with both contributing to transformed growth. PKCɩ-dependent phosphorylation of cytoplasmic ECT2 activates an oncogenic RAC1-PAK-MEK-ERK pathway (18) whereas PKCɩ-mediated phosphorylation of nuclear ECT2 stimulates RAC1-dependent ribosomal DNA (rDNA) transcription (19,20). A similar nuclear ECT2-dependent activation of RAC1 regulates ovarian cancer cell growth (21). In both cancer types, the oncogenic function of ECT2 is separate and distinct from its role in normal cell cytokinesis.

Here, we assessed a driver function for ECT2 in colorectal cancer (CRC). We determined that ECT2 protein levels were elevated in CRC tumor tissue and cell lines through enhanced *ECT2* gene transcription. This increase in transcription was associated with loss of *APC* tumor suppressor function, indicating that ECT2 overexpression is an early event in CRC progression. Immunohistochemical analyses identified elevated nuclear and cytoplasmic ECT2 levels in primary CRC tumor tissue, with both contributing to CRC tumorigenesis. A low cytoplasmic-nuclear (C:N) ratio of ECT2 correlated with poor patient survival. We found that nuclear ECT2 was required for CRC cell growth, in part by activating ribosomal RNA (rRNA) synthesis. Suppression of ECT2 expression impaired anchorage-independent growth and invasion of CRC cell lines. Finally, *Ect2* deficiency increased survival in a *Fapbl-Cre;Apc*$^{2lox14/+}$;*Kras*$^{LSL-G12D/+}$ mouse model of colon cancer. In summary, we determined that overexpression and mislocalization of ECT2 promote its driver function in CRC growth, which is distinct from its role in regulation of normal cell cytokinesis.

Materials and Methods

TCGA data analyses

Colon and rectal adenocarcinoma (COADREAD) TCGA datasets were downloaded from the UCSC Cancer Browser (RRID:SCR_011796) (22), including gene expression (AgilentG4502A_07_03, IlluminaHiSeq), copy number (gistic2, gistic2_thresholded), and clinical data. Briefly, copy number was measured using whole genome microarray. GISTIC2 methods were applied using Firehose (software.broadinstitute.org) to produce gene-level copy number estimates, and were thresholded to −2 (homozygous deletion), −1 (single copy deletion), 0 (diploid), +1 (low-copy number amplification), or +2 (high-copy number amplification). Values were centered to the mean. A CRC dataset (633 cases, http://tcga-data.nci.nih.gov/tcga/, RRID:SCR_003193) was evaluated for correlations between expression of ECT2 and 15 RHOGEFs, and 276 ribosomal processing genes (23) using the Mutual Exclusivity tool (cBioPortal.org, RRID:SCR_014555).

Oncomine analyses

ECT2 expression levels in colorectal adenocarcinomas, adenomas or normal tissue were analyzed using the Oncomine Compendium of Expression Array data (www.oncomine.org; RRID:SCR_007834).

Gene array analysis

RNA was extracted from macrodissected snap-frozen tumor samples using the AllPrep DNA/RNA Kit (Qiagen) and quantified via NanoDrop spectrophotometry (ThermoScientific). RNA quality was assessed by the 2100 Bioanalyzer (Agilent). Similar quality RNA was selected for hybridization using RNA integrity number and by inspection of the 18S and 28S ribosomal RNA. One µg RNA was used as template for cDNA preparation and hybridized to the Human Genome 4×44K Microarray Kit (Agilent). cDNA was labeled with Cy5-dUTP and a reference control (Stratagene) was labeled with Cy3-dUTP using the Low RNA Input Linear Amplification Kit (Agilent) and hybridized overnight at 65°C to the Human Genome Microarray Kit, 4×44K (Agilent). Arrays were washed and scanned using an Agilent scanner (Agilent).

Immunohistochemistry (IHC) for ECT2 in tissue microarrays (TMAs) and full tissue slides

ECT2 antibody validation and the comprehensive protocols are described in Supplementary Materials and Methods. Written informed consent was obtained from all patients. Studies were approved by the human subjects committees at the University of North Carolina at Chapel Hill and the clinical documentation protocol of Charité Universitätsmedizin Berlin.

Ect2 RNA expression and IHC analyses of Villin-Cre[ERT2] *Apc*^{fl/fl} mice

Experiments were performed in accordance with UK Home Office guidelines (Project license 70/8646), adhered to ARRIVE guidelines, and subjected to review by the animal welfare and ethical review board (AWERB) of the University of Glasgow. Alleles used were Villin-Cre[ERT2] (24) and *Apc*[580S] (*Apc*[fl]) (25). Recombination driven by Villin-Cre[ERT2] was induced by one intraperitoneal injection of 80 mg/kg tamoxifen per day for two days to conditionally delete APC specifically in the intestine of Villin-Cre[ERT2] *Apc*^{fl/fl} mice; Villin-Cre[ERT2] *Apc*^{+/+} mice were used as wild-type (WT) controls. Induction was carried out at 6–12 weeks of age, at a minimum weight of 20 grams. Animals were sacrificed four days post induction, with RNA isolated from small intestinal tissue collected 5 cm distal to the stomach. Tissue was dissociated using a Precellys24-homogenizer (Bertin Instruments). RNA was isolated using a RNeasy Mini Kit (Qiagen). Quality and quantity of purified RNA were determined using an Agilent2200 TapeStation with RNA ScreenTape (Agilent). Libraries for cluster generation and DNA sequencing were prepared as described (26), using TruSeq RNA-Sample-Prepv2 (Illumina). Libraries were run on Illumina NextSeq using the High-Output75 cycles kit (2×36 cycles, paired end reads, single index). Fastq files are deposited at European Nucleotide Archive (RRID:SCR_006515), study accession number PRJEB20615. Tissue specimens were fixed in 10% neutral buffered formalin for 12–18 h at 4°C and processed using standard techniques. Sectioned tissue specimens were stained with hematoxylin and eosin (H&E) to aid gross histological assessment, IHC staining to visualize distribution of β-catenin (BD Biosciences, #610154, RRID:AB_397555), or using RNA *in situ* hybridization (RNAscope) targeting *Ect2* mRNA. The *Ect2* targeting RNAscope probe (ACD 502128) was stained using the RNAscope 2.5-LS-Assay-BROWN (ACD) on the BondRX-Multiplex-IHC-Stainer (Leica Biosystems). *Ect2* RNAscope was quantified using Halo software (Indica Labs, RRID:SCR_018350): 20 small intestine crypts/mouse were manually annotated; the *Indica Labs–ISH v3.4.7* algorithm was used to determine the area of *Ect2* staining, normalized to total crypt area.

Additional mouse models

Mouse studies were approved by the University of North Carolina Institutional Animal Care and Use Committee (IACUC). *Apc*[Min/+] mice (25), and Fabpl-[4X@132]-Cre, *Kras*[LSL-G12D/+] *Apc*[lox14/+] (27) and *Ect2*[lox/+] (28) mice were described previously. Mouse euthanasia was performed per IACUC guidelines. The abdomen was opened and gross dissection findings were noted. The intestinal tract was removed and rinsed in PBS. Intestines were opened lengthwise. Polyps were counted, measured and a few were removed and frozen for nucleic acid and protein extractions. The remaining tissue was rolled, fixed in 10% phosphate buffered formalin for histological analysis and paraffin embedded. Sections were stained using H&E and reviewed by a gastrointestinal pathologist (DT) blinded to genotype.

Disease-specific survival was evaluated using the Kaplan-Meier method and significance evaluated using the log-rank test.

Cell lines

COLO-320-HSR (RRID:CVCL_0220), LS-1034 (RRID:CVCL_1382), SNU-C1 (RRID:CVCL_1708), SW48 (RRID:CVCL_1724), T84 (RRID:CVCL_0555), HCT-116 (RRID:CVCL_0291), LOVO (RRID:CVCL_0399), LS-174T (RRID:CVCL_1384), SW480 (RRID:CVCL_0546), SW620 (RRID:CVCL_0547) and HT-29 (RRID:CVCL_0320) were obtained from American Type Culture Collection (ATCC) and included authentication and quality controls. Cells were maintained in DMEM or RPMI-1640 supplemented with 10% FBS and passaged for one month or ten passages before a new aliquot was thawed. Immortalized mouse embryo fibroblasts (MEFs) were derived from mouse embryos that harbor a conditional *Ect2* floxed allele (*Ect2*fl/fl) as described (10). Briefly, Cre-mediated deletion results in a floxed allele lacking exon 8 that is a null mutation based on the complete loss of ECT2 protein expression. Recombinant adenovirus expressing Cre recombinase (Ad-Cre) or green fluorescent protein (Ad-GFP) to control for effects due to adenovirus infection were used to induce loss of ECT2 expression (Gene Transfer Vector Core, University of Iowa). Cells were maintained in a humidified chamber with 5% CO_2 at 37°C. Cells were monitored monthly for *Mycoplasma* contamination using the MycoAlert *Mycoplasma* Detection Kit (Lonza).

ECT2 constructs

Lentiviral ECT2 and control shRNA expression vectors, and the shRNA-resistant cDNA expression vector of full-length WT ECT2 are described in Supplementary Materials and Methods.

β-catenin overexpression and MYC/KRAS knockdown studies

Details are described in Supplementary Materials and Methods.

qPCR mRNA expression analysis

Total RNA was isolated using the RNeasyPlus Mini Kit (QIAGEN) following the manufacturer's protocol. RNA was quantified and converted to cDNA using the High-Capacity cDNA Archive Kit (Applied Biosystems). *ECT2* RNA (Hs00216455_m1 (ABI Assay ID)) and 45S rRNA expression were assessed using TaqMan-Fast-Universal PCR Master Mix (Applied Biosystems). Details for 45s pre-rRNA are: Forward: TCGTCCTCCTCGCTTGC, Reverse: GCAGGATCAACCAGGTAGGTAAG, Reporter: TCGCCGCGCTCTAC. qPCR amplification was performed using the ViiA7 Real-Time PCR Machine (Applied Biosystems). Relative expression values were determined using ubiquitin C (ABI Assay ID Hs00824723_m1) as internal control.

Growth and Matrigel invasion assays

MTT viability assays were performed by plating cells in 96-well plates at 10^3 cells/well and were grown at 37°C for 24–120 h. MTT was dissolved in PBS at 5 mg/ml and 20 μl of MTT solution was added to each well. Plates were incubated at 37°C for 2 h, medium and MTT

solution were removed, and the formazan product produced by living cells was dissolved by adding 100 µl DMSO. After a few minutes at RT to ensure that all crystals were dissolved, plates were read on an ELX800 microplate reader (BioTek Instruments) at 570 nm.

Anchorage-independent soft agar colony formation growth assays were done as described previously (29). Briefly, cells were resuspended in medium supplemented with 0.3% Bacto Agar (BD Biosciences), with 2×10^4 cells plated per well over a 0.6% Bacto Agar layer in 6-well plates. Cells were maintained at 37°C for 2–4 weeks, viable colonies were visualized by staining with MTT for 30 min at 37°C and quantified in three wells per condition. Alternatively, cells were assessed for anchorage-independent growth in agarose (SeaPlaque GTG Agarose, Lonza) to form colonies. Complete 2x medium was mixed with 1.5% agarose to achieve 0.75% final agar concentration in medium plated into 35 mm dishes to create an agar bottom layer. Single cell suspensions containing 5×10^3 cells per plate were mixed in soft agar and dispensed over the solidified bottom layer of soft agar. Plates were incubated at 37°C and colony growth assessed after three weeks. Plates were fixed in methanol for 20 min followed by two PBS washes. Giemsa (EMD Millipore) was diluted (1:20) in PBS and fixed colonies were stained at RT for 2 h. Plates were washed with PBS and imaged using the UVP BioSpectrum Imaging System. Colony size and number were determined using Image-Pro Plus 7 Image Analysis Software (RRID:SCR_016879) (9).

Real-time Matrigel invasion assays were performed on the xCELLigence system (Roche Applied Science). A CIM-Plate16 (Agilent Technologies) was used where the top of the trans-well was coated with Matrigel (BD Bioscience) and allowed to polymerize at 37°C. After 2 h, cells were plated over the Matrigel in serum-free growth medium and complete growth medium supplemented with 10% FBS was added to the bottom of the transwell as a chemoattractant. Invasive cells will migrate through the Matrigel and though the micropores of the CIM-Plate16. Migrating cells were detected by the electronic sensing microelectrodes, producing changes in impedance, reported as cell index values. The xCELLigence system was set to collect impendence data every two minutes for at least 40 h.

Cell cycle analyses

Cells were trypsinized, washed in PBS, fixed in 70% ethanol and stored at −20°C. The day prior to analysis, cells were washed in PBS and stained with 0.5 ml of propidium iodine staining solution (1% Triton-X-100, 1 mg/ml propidium iodine, 100 mg/ml RNAse A) overnight at 4°C. Data were collected on a CyAn ADP Analyzer (Beckman Coulter). Analyzer was equipped with forward and side scatter and nine colors of fluorescence using 405 nm, 488 nm and 635 nm excitations. The ModFit Software (BD Biosciences, RRID:SCR_016106) was used for analysis.

Immunoblotting

Cells were trypsinized, pelleted and washed twice with ice-cold PBS. Cells were lysed in RIPA buffer (10 mM Tris pH 7.5, 150 mM NaCl, 1 mM EDTA, 0.5% Na-deoxycholate, 0.1% SDS and 1% Triton-x100) with phosphatase inhibitor cocktail sets I/II (Calbiochem) and complete protease inhibitor (MilliporeSigma). Murine tissue lysates were prepared using Pierce RIPA buffer as described above and containing phosphatase

inhibitor cocktail sets I/II (Calbiochem) and complete protease inhibitor (MilliporeSigma). Protein lysates were quantitated using BCA. Equal amounts of protein (15 μg) were loaded for each sample, resolved in 4–20% SDS-PAGE (Novex, Life Technologies), and transferred to Immobilin-P polyvinylidene difluoride membrane (MilliporeSigma). Membranes were blocked with 5% milk in phosphate-buffered saline-Tween20, incubated in primary antibodies followed by incubation with HRP-conjugated secondary antibodies. The following antibodies were used: anti-ECT2 antibody (Millipore, #07–1364, RRID:AB_10805932), anti-β-actin antibody (Sigma, #A5441, RRID:AB_476744), anti-vinculin antibody (Sigma, #V9131, RRID:AB_477629), anti-GAPDH antibody (Sigma, #G8795, RRID:AB_1078991; Cell Signaling Technology, #5174, RRID:AB_10622025), anti-HA-tag antibody (Covance, #MMS-101P-200, RRID:AB_10064068), active anti-β-catenin antibody (Cell Signaling Technology, #19807), total anti-β-catenin antibody (Cell Signaling Technology, #8480, RRID:AB_11127855), anti-phospho-MYC S62 antibody (Abcam, #185656), anti-MYC-antibody (Cell Signaling Technology, #5605), anti-KRAS-antibody (Sigma, #WH0003845M1, RRID:AB_1842235), and the HRP-linked goat-anti-rabbit IgG antibody (Cell Signaling Technology, #7074, RRID:AB_2099233) and horse-anti-mouse IgG antibody (Cell Signaling Technology, #7076, RRID:AB_330924). Protein bands were visualized by enhanced chemiluminescence detection (Thermo Fisher Scientific), quantified by densitometric intensity using ImageJ (RRID:SCR_003070) and normalized to loading control.

Immunofluorescence analyses

Cells were seeded on coverslips, after 24 h washed twice with PBS and fixed with 2% paraformaldehyde in PBS for 10 min at RT. After PBS wash, cells were permeabilized with 0.1% Triton X-100 (Sigma) for 5 min at RT followed by blocking using 2% BSA (Sigma) in PBS for 30 min at RT. Cells were incubated with primary antibody for 60 minutes at RT, washed three times with PBS, and incubated with the secondary antibody for 45 min at RT. Cells were washed three times with PBS and mounted with FluorSave Reagent (MilliporeSigma). Endogenous ECT2 was detected with anti-ECT2 antibody (Millipore, #07–1364, RRID:AB_10805932) followed by a goat anti-rabbit secondary antibody conjugated to Alexa-Fluor488 (Invitrogen #A1108). Ectopically expressed HA epitope-tagged ECT2 variants were detected with anti-rabbit HA antibody (Cell Signaling Technology, #3724, RRID:AB_1549585) followed by a goat anti-rabbit secondary antibody conjugated to Alexa-Fluor488 (Invitrogen #A1108). To visualize F-actin, cells were stained with phalloidin labelled with Alexa-Fluor647 (Invitrogen, #A22287). The nucleus was visualized using 5 ng/ml DAPI (Invitrogen, #D3571) in PBS. Images were acquired on an BX61 fluorescence microscope (Olympus).

Statistical analyses

Statistical analyses are detailed in the specific method subsection. Data are shown as mean ± SD or SEM as indicated. Statistical analyses were performed using Prism (GraphPad, RRID:SCR_002798) or Microsoft Office statistical tools. Briefly, comparisons between groups were performed using paired or unpaired Student t test or Fisher's Exact Test (TCGA data analyses), two-tailed Mann-Whitney test (RNA-seq analyses, H & E analyses) and survival curves were evaluated using the Kaplan-Meier method and the log-rank test.

Statistical methods used in the IHC studies are explained in detail in IHC method part. P < 0.05 was considered as statistically significant. P values were as indicated in the figure or denoted by *, P < 0.05; **, P < 0.01; *** P < 0.001; ****, P < 0.0001. For in vivo studies, sample sizes and animal numbers were determined from pilot laboratory studies and published literature. Mice were excluded if they were euthanized due to health reasons unrelated to tumor growth.

Results

Increased ECT2 gene and protein expression in CRC is associated with APC loss

To identify genes deregulated in CRC, we performed gene microarray analyses of human CRC tumor and unmatched non-tumor tissues. We found increased expression levels of the *ECT2* gene in CRC tumors (Fig. 1A). To further validate these results, we analyzed seven published gene microarray datasets (30–34) using the Oncomine database and found increased *ECT2* mRNA expression in both colon and rectal adenoma, and in adenocarcinoma (Supplementary Fig. S1A). Similarly, our analyses of TCGA data of Agilent gene expression arrays of 224 CRC and 22 paired normal tissue samples (Fig. 1B) and of RNA-Seq analyses of 380 CRC and 50 paired normal tissue samples (Fig. 1C) revealed elevated *ECT2* mRNA expression in CRC tumors. However, the GISTIC analysis of 615 CRC samples showed that the *ECT2* gene copy number was infrequently increased (Fig. 1D). Thus, *ECT2* mRNA overexpression is not associated with *ECT2* gene amplification in CRC (Supplementary Fig. S1B). This contrasts with squamous cell carcinoma and ovarian serous carcinoma where increased *ECT2* expression was driven by copy number gain (CNG) of the *ECT2* gene as part of a recurrent 3q26 amplicon (18,21,35).

To determine whether increased *ECT2* mRNA abundance resulted in elevated ECT2 protein expression in CRC tumors, we analyzed protein levels in a panel of matched normal, primary and metastatic CRC tissue. We observed increased protein expression of ECT2 in six of eight primary CRC tumors and in six of eight metastatic tumors when compared with adjacent normal tissue (Fig. 1E). Additionally, we observed high ECT2 protein expression in nine of 10 human CRC cell lines (Fig. 1F).

The loss of the tumor suppressor *APC* is an early event in CRC tumor progression. To investigate whether *Apc* loss is associated with *Ect2* gene expression, we applied RNA-seq analysis to whole intestines of WT and Villin-Cre^ERT2 *Apc*^fl/fl mice. We observed that *Ect2* gene expression was highly upregulated following targeted deletion of *Apc* in the intestinal epithelium (Fig. 1G). To visually assess the localization of *Ect2* expression, RNAscope staining was performed in the same model. We found that *Ect2* expression was restricted to the crypts of the intestinal epithelium in WT tissue and substantially increased upon loss *Apc* loss, while crypt localization was maintained (Fig. 1H and 1I, Supplementary Fig. S1C). Increased *Ect2* expression appeared coincident with nuclear accumulation of β-catenin following *Apc* loss (Fig. 1H). Critically, while the RNA-seq analysis (Fig. 1G) was carried out on whole tissue (including stroma), the RNAscope study indicated that *Ect2* expression was epithelial-specific in the intestine (Fig. 1H; Supplementary Fig. S1C). Furthermore, we found elevated Ect2 protein levels in benign adenomas derived from the *Apc*^Min/+ mouse that harbors a germline nonsense mutation at codon 850 resulting

in expression of a truncated APC protein (Fig. 1J; Supplementary Fig. S1D). These data support increased ECT2 expression as an early event in CRC development and association with loss of *APC* function.

Our evaluation of *APC* mutation status also found a correlation between the presence of an *APC* mutation and high ECT2 expression in nine of 10 human CRC cell lines; only one cell line (LS-174T) has high ECT2 expression and is APC WT (Fig. 1F, Supplementary Table S1). To address a role for *APC* loss-mediated signaling in driving ECT2 expression, we ectopically expressed constitutively activated β-catenin (S33A/S37A/T41A/S45A; 4A) in the *APC* WT HCT-116 cell line with low ECT2 expression (Supplementary Fig. S1E). As expected, activated β-catenin increased MYC levels, but no significant increase in ECT2 expression was detected. Thus, perhaps an activity caused by *APC* loss of function independent of canonical β-catenin and MYC activation may be involved in ECT2 regulation.

In contrast to *APC*, *KRAS* mutation status was not correlated with ECT2 expression levels. The three *KRAS* WT cell lines showed similar high ECT2 levels as the six KRAS-mutant lines, while one *KRAS*-mutant line (HCT-116) had low ECT2 levels (Fig. 1F, Supplementary Table S1). Similarly, a recent IHC analysis of 34 CRC tumors revealed no correlation between *KRAS* mutation status and ECT2 protein expression in early adenomas and carcinomas (36). However, since both *APC* loss and subsequent β-catenin activation, and *KRAS* mutation, can cause increased MYC expression, we addressed a possible role for MYC in driving ECT2 expression. We found that siRNA-mediated depletion of *MYC* in the KRAS-mutant *APC* WT cell line HCT-116 decreased rather than increased ECT2 levels (Supplementary Fig. S1F), whereas suppression of *MYC* or *KRAS* did not alter ECT2 levels in the *KRAS*-mutant *APC*-mutant cell line SW480 (Supplementary Fig. S1G). In summary, our data indicate that the elevated gene and protein expression of ECT2 in CRC can be induced by APC-dependent and APC/β-catenin/MYC-independent mechanisms that remain to be elucidated.

Cytoplasmic mislocalization and increased nuclear levels of ECT2 contribute to the early events of CRC tumorigenesis and poor survival

In addition to ECT2 overexpression, deregulated subcellular localization of nuclear ECT2 was linked to aberrant ECT2 function in transformed mouse fibroblasts (17) and in human lung and ovarian cancer (18,21). To determine if cytoplasmic mislocalization of ECT2 is associated with CRC, we first analyzed expression and subcellular localization of ECT2 in tissue microarrays of a cohort of 146 patients with available ECT2 expression levels (scores) for normal, CRC tumor tissue or both. Clinico-pathologic characteristics and overall survival are summarized in Supplementary Table S2. We performed IHC (Supplementary Fig. S2A and 2B) using an anti-ECT2 antibody that we first validated for this method (Supplementary Fig. S2C). Representative images of normal colorectal tissues compared to CRC tumor sections illustrating different expression levels of ECT2 are shown in Fig. 2A. We found a strong trend of elevated levels of both nuclear and cytoplasmic ECT2 in CRC tumors compared to matched normal tissue (Fig. 2B). Importantly, the ratio of cytoplasmic:nuclear (C:N) ECT2 was significantly higher in CRC tumors than in normal tissue ($P = 0.01$, Fig.

2C) indicating that tumors displayed cytoplasmic mislocalization of ECT2 whereas normal tissue did not. Nevertheless, total ECT2 protein levels were still significantly higher in the nucleus compared to the cytoplasm in all tissues (51.1±3.6 in the nucleus versus 29.1±2.6 in the cytoplasm; average of tumor and normal nuclear scores ± SEM, $P < 0.001$). To better understand the relationships between total expression and subcellular localization of ECT2 and the development and outcomes of CRC, we undertook additional analyses.

To investigate whether cytoplasmic mislocalization and elevated nuclear levels of ECT2 occur in the earliest stages of CRC tumor development, we analyzed an independent cohort of 16 matched adenoma-carcinoma samples which were localized directly adjacent to each other (36). Similar to the larger carcinoma cohort, we found significantly higher levels of nuclear and cytoplasmic ECT2 in the areas of carcinoma, with strongly increased levels even in early adenomas (Fig. 2D and 2E, Supplementary Fig S2D). In particular, nuclear ECT2 was already greatly elevated in adenomas, consistent with our findings of elevated ECT2 in early mouse adenomas induced upon loss of *Apc* (Fig. 1G). Furthermore, upon close inspection of each individual sample, a high level of heterogeneity within the normal compartment became evident. While ECT2 was minimally expressed in most normal tissue, it was elevated in hyperplastic and lesional foci in close proximity to areas of high-grade dysplasia / early intramucosal adenocarcinoma (Supplementary Fig. S2D).

We next assessed the relationship between ECT2 protein levels and clinico-pathologic characteristics. We found that nuclear, but not cytoplasmic, ECT2 expression correlated with the evaluated characteristics such as tumor grade. Well-differentiated tumors exhibited low levels of nuclear ECT2, but as the tumor grade increased to poorly differentiated, nuclear expression of ECT2 increased ($P = 0.04$) (Table 1). Despite this, neither nuclear or cytoplasmic ECT2 alone nor the sum of them correlated with overall survival (Supplementary Fig. S2E and 2F). Instead, a lower C:N ratio of ECT2 did show a significant association with poor survival (Fig. 2F) indicating a key role of the elevated nuclear ECT2 in CRC progression. These data also suggest that the intracellular re-distribution of ECT2 in CRC tumors may be a more reliable predictive biomarker of CRC prognosis than total ECT2 or the levels in either compartment alone. To address this possibility, we applied Cox proportional hazards models to the clinico-pathologic data. In the univariate model, a higher C:N ECT2 ratio was significantly associated with a lower risk of death: as the ratio increased by 0.5 increments, the risk of death decreased by 40% (Supplementary Table S3). Even after adjustment for age, stage, differentiation and location of the tumor, and prior chemotherapy, higher C:N ECT2 ratios were associated with a statistically significant reduced risk of dying. Thus, with respect to nuclear ECT2, worse survival was associated with lower C:N ratios, i.e., with higher proportions of ECT2 localized to the nucleus.

ECT2 promotes CRC anchorage-independent growth and invasion

We next assessed the role of ECT2 overexpression in supporting CRC growth. Utilizing two validated lentiviral *ECT2* shRNA vectors (18), we successfully depleted ECT2 expression in multiple human CRC cell lines (Fig. 3A). Suppression of ECT2 did not significantly perturb anchorage-dependent cell proliferation (Fig. 3B) or alter cell cycle progression such as accumulation in the G2/M phase (Fig. 3C), indicating that loss of ECT2 did not

impair cytokinesis of these tumor cell lines. In contrast, we observed a significant reduction in anchorage-independent growth, as determined by colony formation in soft agar (Fig. 3D), and in invasion through Matrigel (Fig. 3E). Thus, similar to lung, brain and ovarian cancer cells (18,21,37), ECT2 functions as a driver of CRC tumor cell growth and invasion independent of its role in regulating normal cell cytokinesis.

Ect2 loss extends survival in a *Kras* and *Apc* driven colon cancer mouse model

We next evaluated a role for ECT2 overexpression in promoting CRC progression *in vivo*. We recently utilized a conditional *Ect2*-deficient mouse to demonstrate a role for ECT2 in $Kras^{G12D}/Trp53^{fl/fl}$-driven lung tumor formation (19). To apply this approach in CRC, we crossed $Ect2^{fl/fl}$ mice with $Fabpl$-$Cre;Kras^{LSL-G12D/+}$ $Apc^{2lox14/+}$ (FAK) mice that develop CRC and have an average survival of 14 weeks (27). FAK mice with heterozygous loss of $Ect2$ ($Ect2^{fl/+}$) had a median disease-specific survival (DSS) of 12.0 weeks whereas mice with homozygous loss of $Ect2$ ($Ect2^{fl/fl}$) had a median DSS of 24.6 weeks (Fig. 4A). The prolonged survival of mice with homozygous *Ect2* loss was due to increased latency of polyp formation and of intramucosal (IM) and invasive (INV) cancers (Fig. 4B and 4C). We observed significantly fewer polyps in mice with homozygous *Ect2* loss than in mice with heterozygous *Ect2* loss (Supplementary Fig. S3A and S3B). These observations support a role for ECT2 overexpression in CRC progression *in vivo*.

Nuclear ECT2 stimulates rRNA expression and is required for CRC transformed growth

Since our IHC analyses (Fig. 2) found that decreased C:N ratio of ECT2 was associated with poorer outcome of CRC patients, we sought to directly address whether nuclear localization of ECT2 is required for transformed growth of CRC cells. Consistent with our observations in primary CRC tumors (Fig. 2), immunofluorescence microscopy analysis detected both nuclear and cytoplasmic pools of endogenous ECT2 in CRC cell lines (Supplementary Fig. S4A).

To assess the importance of ECT2 structural elements in the ability to support CRC growth, we generated hemagglutinin (HA) epitope-tagged ECT2 WT and mutant constructs (Fig. 5A). Each *ECT2* allele was stably expressed in HT-29 cells, either alone or together with *ECT2* shRNA to suppress endogenous ECT2 (Fig. 5B, Supplementary Fig. S4B). We found that ectopic expression of WT full-length ECT2 rescued the anchorage-independent cell growth defect caused by suppression of endogenous ECT2 (Supplementary Fig. S4C). Mutation of one NLS alone (N1 or N2) resulted in partial loss of nuclear localization, whereas mutation of both NLS sequences (N3) caused near-complete loss of nuclear ECT2 (Fig. 5C). These data indicate that both NLS sequences contribute to control nuclear ECT2 localization. Expression of either N1 or N2, but not N3, ECT2 partially restored the impaired anchorage-independent cell growth caused by depletion of endogenous ECT2 (Fig. 5D). However, the N3 mutant in which both NLS motifs are mutated was expressed to a lesser extent than N1, N2 or WT. ECT2 harboring a mutated DH domain did not restore cell growth, indicating that the RHOGEF catalytic activity is required for ECT2-mediated anchorage-independent growth (Supplementary Fig. S4C). In summary, efficient nuclear localization and RHOGEF activity are important for ECT2-mediated support of CRC anchorage-independent growth.

Interestingly, although our previous study found that the sequences carboxyl-terminal to the DH-PH domains were required for growth and morphologic transformation of NIH/3T3 mouse fibroblasts (38), these sequences and the PH domain itself were both dispensable for ECT2-dependent anchorage-independent growth of human CRC cells (Supplementary Fig. S4C). Our results in CRC also contrast with previous studies in NIH/3T3 cells where mutation of the NLS motifs was sufficient to cause activation of full-length ECT2 transforming activity (17), indicating that immortalized mouse fibroblasts can be transformed by ECT2 functions that are not seen in established human colonic epithelial cancer cells. Consistent with this, although the cytoplasmic, constitutively activated N-ECT2 protein exhibits potent transforming activity in NIH/3T3 mouse fibroblasts (14,17,38), truncated ECT2 proteins have not been described in human cancers. To further explore this distinction, we next attempted to evaluate the activity of the N-ECT2 truncated protein in CRC cells. When we utilized a lentivirus-based puromycin resistant cDNA expression vector encoding N-ECT2, we failed to isolate puromycin-resistant stable populations of multiple CRC cell lines (HCT-116, HT-29, and SW620) that ectopically expressed this truncated protein. The few cells that did arise displayed altered cellular morphology, and were rounded and poorly adherent, suggesting induction of apoptosis (Fig. 5E; Supplementary Fig. S4D). Although we were unable to verify the basis for this growth suppression since there were insufficient cells available to analyze, this result may help explain why N-terminally truncated ECT2 has not been observed in human cancers.

We recently showed that nuclear ECT2 regulation of ribosomal RNA (rRNA) synthesis in lung adenocarcinoma is essential for tumor growth (19,20,39). To determine if ECT2 facilitates rRNA synthesis in CRC, we interrogated the TCGA human CRC dataset of 633 tumors. Similar to our findings in lung cancer, we found a significant and specific correlation between expression of *ECT2*, but not other RHOGEFs, and a majority of genes critical to ribosome biogenesis (Fig. 6A and 6B). Furthermore, we observed that shRNA-mediated suppression of ECT2 in three CRC cell lines (Fig. 6C and 6D) impaired both rRNA expression (Fig. 6E) and anchorage-independent growth (Fig. 6F). In summary, our findings indicate that nuclear ECT2 acts as a driver in CRC, in part through stimulation of rRNA expression.

Nuclear ECT2 is not required for normal cell cytokinesis

We show here that ECT2 functions as a cancer driver independent of regulating cytokinesis in CRC cells (Fig. 3C). However, in addition to its role in cancer, ECT2 is well known to control cytokinesis in normal cells (28,40–42), which requires ECT2 to interact with the plasma membrane through its carboxyl-terminal sequences (43,44). However, the function of the NLS motifs has not been addressed. We investigated whether nuclear localization of ECT2 is also required for normal cell cytokinesis. We have shown previously that *Ect2* is essential for normal cell cytokinesis in immortalized MEFs established from *Ect2*$^{fl/fl}$ mice (28). We therefore stably expressed HA-tagged ECT2 and mutants in these MEFs, prior to infection with adenoviral Cre (Ad-Cre) to deplete endogenous *Ect2* (Fig. 7A). Cell cycle analyses showed that depletion of endogenous ECT2 disrupted cytokinesis, as indicated by accumulation of cells in the G2/M phase (Fig. 7B). This is line with observations by ourselves and others that ECT2 function is essential for cytokinesis in non-transformed

cell types (19,28). Re-expression of ECT2 WT rescued the cytokinesis defect as indicated by a similar percentage of cells in G2/M in control and ECT2 depleted cells (Fig. 7B). Importantly, expression of ECT2 variants with inactivating mutations of the first (N1) or both (N3) NLS motifs also restored cytokinesis even though they are mislocalized from the nucleus into the cytoplasm (Fig. 7C). Thus, ECT2 nuclear localization is essential for its function as a cancer driver but not for its role in normal cell cytokinesis. Finally, consistent with previous findings that RHOA activation is important for cytokinesis (28,40,41), the RHOGEF-inactive ECT2 mutant (DH) did not restore cytokinesis. We also observed that the C and PH mutants did not rescue the cytokinesis defect, similar to human cervical carcinoma cells (43,44). In summary, our data indicate that the NLS motifs of ECT2 and thus its nuclear localization, while essential for driving CRC growth, are not required for ECT2 function in normal cell cytokinesis.

Discussion

The RHOGEF ECT2, an activator of the small GTPase RHOA, was identified initially as an oncogene in the same NIH/3T3 fibroblast assays that discovered the RAS oncogenes in cancer (14). The oncogenic function of ECT2 in these assays was caused by amino-terminal truncation. However, this was due to *in vitro* DNA manipulation and truncated ECT2 proteins have not been found in human cancers. Instead, overexpression of full-length ECT2 has been described for multiple cancers including glioblastoma, lung, ovarian, esophageal and gastric cancers (18,21,45–48). In the present study, we identified a driver role for ECT2 overexpression, nuclear function, and cytoplasmic mislocalization in CRC.

We found increased ECT2 protein levels in both the nucleus and the cytoplasm of CRC tumor tissue and human CRC lines. This increase is driven by enhanced *ECT2* gene transcription, rather than by gene amplification as described in lung squamous cell carcinoma and ovarian serous carcinoma (18,21). Increased *ECT2* gene expression was associated with loss of the tumor suppressor APC, one of the earliest events of CRC tumorigenesis, and indeed we found increased ECT2 in early adenomas in both human and mouse colons. We observed increased Ect2 expression upon loss of *Apc* function in two distinct mouse models of CRC development, and this was associated with elevated β-catenin, the major consequence of *Apc* loss-of-function. However, exogenous expression of constitutively active β-catenin did not increase ECT2 expression in established human CRC cell lines. Thus, whether *APC* loss, in particular through the canonical β-catenin pathway, is a key mechanistic basis for ECT2 upregulation in established human CRC remains to be fully elucidated.

As we observed previously in lung and ovarian cancer (19–21), elevated ECT2 levels in both cytoplasmic and nuclear compartments drive CRC growth, through distinct mechanisms. CRC tumors are characterized by an increased C:N ratio of ECT2 compared to normal tissue, indicating mislocalization of nuclear ECT2 into the cytoplasm, similar to what we have described in lung (18) and ovarian cancer (21). In those cancers, mislocalized cytoplasmic ECT2 interacts with the PKCι-Par6 complex, and through PKCι-mediated phosphorylation, drives a proliferative RAC1-MEK-ERK signaling axis which is required for transformed growth (18,49). Since our data indicate that ECT2 has a similar role in

CRC as in lung and ovarian cancer, PKCι may control ECT2 function also in CRC. This hypothesis is further supported by our finding that deletion of the amino-terminal regions of ECT2 (ΔN-ECT2) inhibited CRC cell growth. ΔN-ECT2 lacks not only the NLS domains but also the BRCT domains which contain the PKCι-mediated phosphorylation T328 site that is required for association of ECT2 with the PKCι-Par6 complex (18,49). Our observation that amino-terminally truncated ECT2 lacking both of these domains is growth-inhibitory may provide an explanation for why such proteins have not been found in human epithelial cell-derived cancers (10,11).

In addition to the cytoplasmic mislocalization of ECT2, we found that nuclear ECT2 contributes strongly to its oncogenic function in CRC. First, although both cytoplasmic and nuclear ECT2 levels are elevated in CRC, the strongest increase has been observed for nuclear ECT2 in early adenomas and carcinomas. Second, lower C:N ratios of ECT2 correlated with poorer CRC patient survival. Third, disruption of the nuclear localization of ECT2 impaired its ability to promote CRC cell growth and invasion. Finally, nuclear ECT2 promotes rRNA transcription in CRC, which occurs predominantly in subset of CRC tumor cells of a defined niche that is located immediately adjacent to the stroma (50). Nuclear ECT2 promotion of rRNA transcription was also identified in lung cancer (19,20,39), suggesting that this pathway may be generally relevant to ECT2-driven transformation. Collectively, these findings suggest that, while both cytoplasmic and nuclear ECT2 are required for cellular transformation, nuclear ECT2 could be particularly important for more aggressive, highly proliferative CRC tumors.

In contrast to transformation, nuclear localization is dispensable for ECT2 function in normal cytokinesis. ECT2 overall is dispensable for cytokinesis in cancer cells whereas ECT2-mediated activation of RHOA signaling is required for normal cell cytokinesis (28,40–42). Cytokinesis defects can, but do not always, induce tumorigenesis (51). It has been shown for multiple cancers including CRC (this study), lung and ovarian cancer (18,21) that ECT2-dependent cancer cell growth is distinct and separate from ECT2 function in cytokinesis. In line with this, some cancer-associated ECT2 mutations have been identified as loss-of-function alterations (52). It is tempting to speculate that, in contrast to normal cells, uncoupling of cell growth and cytokinesis could be a general feature of ECT2 overexpression in cancer, which raises the question of how those cancer cells are then dividing.

In summary, our studies provide evidence that ECT2, a protein essential for cytokinesis, acquires a driver role early in CRC tumorigenesis by a mechanism independent of its function in cytokinesis. Our findings underscore the importance of tightly regulated subcellular localization of ECT2 in normal and neoplastic cell biology. ECT2 may have a unique oncogenic driver role in human carcinogenesis because it is only one of two Dbl RHOGEFs with nuclear localization and it possesses domains (e.g., BRCT) not found in any other DBL family RHOGEFs. Finally, our findings may provide a foundation to identify new molecular determinants for CRC diagnosis and therapy.

Supplementary Material

Refer to Web version on PubMed Central for supplementary material.

Acknowledgments

References

1. Clayton NS, Ridley AJ. Targeting Rho GTPase Signaling Networks in Cancer. Front Cell Dev Biol 2020;8:222. [PubMed: 32309283]

2. Hodge RG, Schaefer A, Howard SV, Der CJ. RAS and RHO family GTPase mutations in cancer: twin sons of different mothers? Crit Rev Biochem Mol Biol 2020:1–22.

3. Lawson CD, Ridley AJ. Rho GTPase signaling complexes in cell migration and invasion. J Cell Biol 2017;217:447–57. [PubMed: 29233866]

4. Zandvakili I, Lin Y, Morris JC, Zheng Y. Rho GTPases: Anti- or pro-neoplastic targets? Oncogene 2017;36:3213–22. [PubMed: 27991930]

5. Hobbs GA, Der CJ, Rossman KL. RAS isoforms and mutations in cancer at a glance. J Cell Sci 2016;129:1287–92. [PubMed: 26985062]

6. Moore AR, Rosenberg SC, McCormick F, Malek S. RAS-targeted therapies: is the undruggable drugged? Nat Rev Drug Discov 2020;19:533–52. [PubMed: 32528145]

7. Bustelo XR. RHO GTPases in cancer: known facts, open questions, and therapeutic challenges. Biochem Soc Trans 2018;46:741–60. [PubMed: 29871878]

8. Cannon AC, Uribe-Alvarez C, Chernoff J. RAC1 as a Therapeutic Target in Malignant Melanoma. Trends Cancer 2020;6:478–88. [PubMed: 32460002]

9. Zhang H, Schaefer A, Wang Y, Hodge RG, Blake DR, Diehl JN, et al. Gain-of-Function RHOA Mutations Promote Focal Adhesion Kinase Activation and Dependency in Diffuse Gastric Cancer. Cancer Discov 2020;10:288–305. [PubMed: 31771969]

10. Cook DR, Rossman KL, Der CJ. Rho guanine nucleotide exchange factors: regulators of Rho GTPase activity in development and disease. Oncogene 2014;33:4021–35. [PubMed: 24037532]

11. Vigil D, Cherfils J, Rossman KL, Der CJ. Ras superfamily GEFs and GAPs: validated and tractable targets for cancer therapy? Nat Rev Cancer 2010;10:842–57. [PubMed: 21102635]

12. Hodge RG, Ridley AJ. Regulating Rho GTPases and their regulators. Nat Rev Mol Cell Biol 2016;17:496–510. [PubMed: 27301673]

13. Eva A, Aaronson SA. Isolation of a new human oncogene from a diffuse B-cell lymphoma. Nature 1985;316:273–5. [PubMed: 3875039]

14. Miki T, Smith CL, Long JE, Eva A, Fleming TP. Oncogene ect2 is related to regulators of small GTP-binding proteins. Nature 1993;362:462–5. [PubMed: 8464478]

15. Katzav S, Martin-Zanca D, Barbacid M. vav, a novel human oncogene derived from a locus ubiquitously expressed in hematopoietic cells. The EMBO Journal 1989;8:2283. [PubMed: 2477241]

16. Cox AD, Der CJ. Ras history: The saga continues. Small GTPases 2010;1:2–27. [PubMed: 21686117]

17. Sai Saito, Liu X-F, Kamijo K, Raziuddin R, Tatsumoto T, Okamoto I, et al. Deregulation and mislocalization of the cytokinesis regulator ECT2 activate the Rho signaling pathways leading to malignant transformation. J Biol Chem 2004;279:7169–79. [PubMed: 14645260]

18. Justilien V, Fields AP. Ect2 links the PKCiota-Par6alpha complex to Rac1 activation and cellular transformation. Oncogene 2009;28:3597–607. [PubMed: 19617897]

19. Justilien V, Ali SA, Jamieson L, Yin N, Cox AD, Der CJ, et al. Ect2-dependent rRNA synthesis Is required for KRAS-TRP53-driven lung adenocarcinoma. Cancer Cell 2017;31:256–69. [PubMed: 28110998]

20. Justilien V, Lewis KC, Meneses KM, Jamieson L, Murray NR, Fields AP. Protein kinase Ciota promotes UBF1-ECT2 binding on ribosomal DNA to drive rRNA synthesis and transformed growth of non-small-cell lung cancer cells. J Biol Chem 2020;295:8214–26. [PubMed: 32350115]

21. Huff LP, Decristo MJ, Trembath D, Kuan PF, Yim M, Liu J, et al. The role of Ect2 nuclear RhoGEF activity in ovarian cancer cell transformation. Genes Cancer 2013;4:460–75. [PubMed: 24386507]

22. Zhu J, Sanborn JZ, Benz S, Szeto C, Hsu F, Kuhn RM, et al. The UCSC Cancer Genomics Browser. Nat Methods 2009;6:239–40. [PubMed: 19333237]

23. Tafforeau L, Zorbas C, Langhendries JL, Mullineux ST, Stamatopoulou V, Mullier R, et al. The complexity of human ribosome biogenesis revealed by systematic nucleolar screening of Pre-rRNA processing factors. Mol Cell 2013;51:539–51. [PubMed: 23973377]

24. el Marjou F, Janssen KP, Chang BH, Li M, Hindie V, Chan L, et al. Tissue-specific and inducible Cre-mediated recombination in the gut epithelium. Genesis 2004;39:186–93. [PubMed: 15282745]

25. Sansom OJ, Meniel VS, Muncan V, Phesse TJ, Wilkins JA, Reed KR, et al. Myc deletion rescues Apc deficiency in the small intestine. Nature 2007;446:676–9. [PubMed: 17377531]

26. Fisher S, Barry A, Abreu J, Minie B, Nolan J, Delorey TM, et al. A scalable, fully automated process for construction of sequence-ready human exome targeted capture libraries. Genome Biol 2011;12:R1. [PubMed: 21205303]

27. Haigis KM, Kendall KR, Wang Y, Cheung A, Haigis MC, Glickman JN, et al. Differential effects of oncogenic K-Ras and N-Ras on proliferation, differentiation and tumor progression in the colon. Nat Genet 2008;40:600–8. [PubMed: 18372904]

28. Cook DR, Solski PA, Bultman SJ, Kauselmann G, Schoor M, Kuehn R, et al. The ect2 rho Guanine nucleotide exchange factor is essential for early mouse development and normal cell cytokinesis and migration. Genes Cancer 2011;2:932–42. [PubMed: 22701760]

29. Cox AD, Der CJ. Biological assays for cellular transformation. Methods Enzymol 1994;238:277–94. [PubMed: 7799794]

30. Ki DH, Jeung HC, Park CH, Kang SH, Lee GY, Lee WS, et al. Whole genome analysis for liver metastasis gene signatures in colorectal cancer. Int J Cancer 2007;121:2005–12. [PubMed: 17640062]

31. Kaiser S, Park YK, Franklin JL, Halberg RB, Yu M, Jessen WJ, et al. Transcriptional recapitulation and subversion of embryonic colon development by mouse colon tumor models and human colon cancer. Genome Biol 2007;8:R131. [PubMed: 17615082]

32. Sabates-Bellver J, Van der Flier LG, de Palo M, Cattaneo E, Maake C, Rehrauer H, et al. Transcriptome profile of human colorectal adenomas. Mol Cancer Res 2007;5:1263–75. [PubMed: 18171984]

33. Skrzypczak M, Goryca K, Rubel T, Paziewska A, Mikula M, Jarosz D, et al. Modeling oncogenic signaling in colon tumors by multidirectional analyses of microarray data directed for maximization of analytical reliability. PLoS One 2010;5.

34. Hong Y, Downey T, Eu KW, Koh PK, Cheah PY. A 'metastasis-prone' signature for early-stage mismatch-repair proficient sporadic colorectal cancer patients and its implications for possible therapeutics. Clin Exp Metastasis 2010;27:83–90. [PubMed: 20143136]

35. Murata Y, Minami Y, Iwakawa R, Yokota J, Usui S, Tsuta K, et al. ECT2 amplification and overexpression as a new prognostic biomarker for early-stage lung adenocarcinoma. Cancer Sci 2014;105:490–7. [PubMed: 24484057]

36. Mamlouk S, Simon T, Tomas L, Wedge DC, Arnold A, Menne A, et al. Malignant transformation and genetic alterations are uncoupled in early colorectal cancer progression. BMC Biol 2020;18:116. [PubMed: 32895052]

37. Weeks A, Okolowsky N, Golbourn B, Ivanchuk S, Smith C, Rutka JT. ECT2 and RASAL2 mediate mesenchymal-amoeboid transition in human astrocytoma cells. The American Journal of Pathology 2012;181:662–74. [PubMed: 22683310]

38. Solski PA, Wilder RS, Rossman KL, Sondek J, Cox AD, Campbell SL, et al. Requirement for C-terminal sequences in regulation of Ect2 guanine nucleotide exchange specificity and transformation. J Biol Chem 2004;279:25226–33. [PubMed: 15073184]

39. Justilien V, Lewis KC, Murray NR, Fields AP. Oncogenic Ect2 signaling regulates rRNA synthesis in NSCLC. Small GTPases 2019;10:388–94. [PubMed: 28657426]

40. Basant A, Glotzer M. Spatiotemporal Regulation of RhoA during Cytokinesis. Curr Biol 2018;28:R570–R80. [PubMed: 29738735]

41. Bement WM, Leda M, Moe AM, Kita AM, Larson ME, Golding AE, et al. Activator-inhibitor coupling between Rho signalling and actin assembly makes the cell cortex an excitable medium. Nat Cell Biol 2015;17:1471–83. [PubMed: 26479320]

42. Gomez-Cavazos JS, Lee KY, Lara-Gonzalez P, Li Y, Desai A, Shiau AK, et al. A Non-canonical BRCT-Phosphopeptide Recognition Mechanism Underlies RhoA Activation in Cytokinesis. Curr Biol 2020;30:3101–15 e11. [PubMed: 32619481]

43. Kotynkova K, Su KC, West SC, Petronczki M. Plasma membrane association but not midzone recruitment of RhoGEF ECT2 Is essential for cytokinesis. Cell Rep 2016;17:2672–86. [PubMed: 27926870]

44. Su KC, Takaki T, Petronczki M. Targeting of the RhoGEF Ect2 to the equatorial membrane controls cleavage furrow formation during cytokinesis. Dev Cell 2011;21:1104–15. [PubMed: 22172673]

45. Hirata D, Yamabuki T, Miki D, Ito T, Tsuchiya E, Fujita M, et al. Involvement of epithelial cell transforming sequence-2 oncoantigen in lung and esophageal cancer progression. Clin Cancer Res 2009;15:256–66. [PubMed: 19118053]

46. Jin Y, Yu Y, Shao Q, Ma Y, Zhang R, Yao H, et al. Up-regulation of ECT2 is associated with poor prognosis in gastric cancer patients. Int J Clin Exp Pathol 2014;7:8724–31. [PubMed: 25674238]

47. Salhia B, Tran NL, Chan A, Wolf A, Nakada M, Rutka F, et al. The guanine nucleotide exchange factors trio, Ect2, and Vav3 mediate the invasive behavior of glioblastoma. The American journal of pathology 2008;173:1828–38. [PubMed: 19008376]

48. Sano M, Genkai N, Yajima N, Tsuchiya N, Homma J, Tanaka R, et al. Expression level of ECT2 proto-oncogene correlates with prognosis in glioma patients. Oncol Rep 2006;16:1093–8. [PubMed: 17016598]

49. Justilien V, Jameison L, Der CJ, Rossman KL, Fields AP. Oncogenic activity of Ect2 is regulated through protein kinase C iota-mediated phosphorylation. J Biol Chem 2011;286:8149–57. [PubMed: 21189248]

50. Morral C, Stanisavljevic J, Hernando-Momblona X, Mereu E, Alvarez-Varela A, Cortina C, et al. Zonation of Ribosomal DNA Transcription Defines a Stem Cell Hierarchy in Colorectal Cancer. Cell Stem Cell 2020;26:845–61 e12. [PubMed: 32396863]

51. Lens SMA, Medema RH. Cytokinesis defects and cancer. Nat Rev Cancer 2019;19:32–45. [PubMed: 30523339]

52. Chen M, Pan H, Sun L, Shi P, Zhang Y, Li L, et al. Structure and regulation of human epithelial cell transforming 2 protein. Proc Natl Acad Sci U S A 2020;117:1027–35. [PubMed: 31888991]
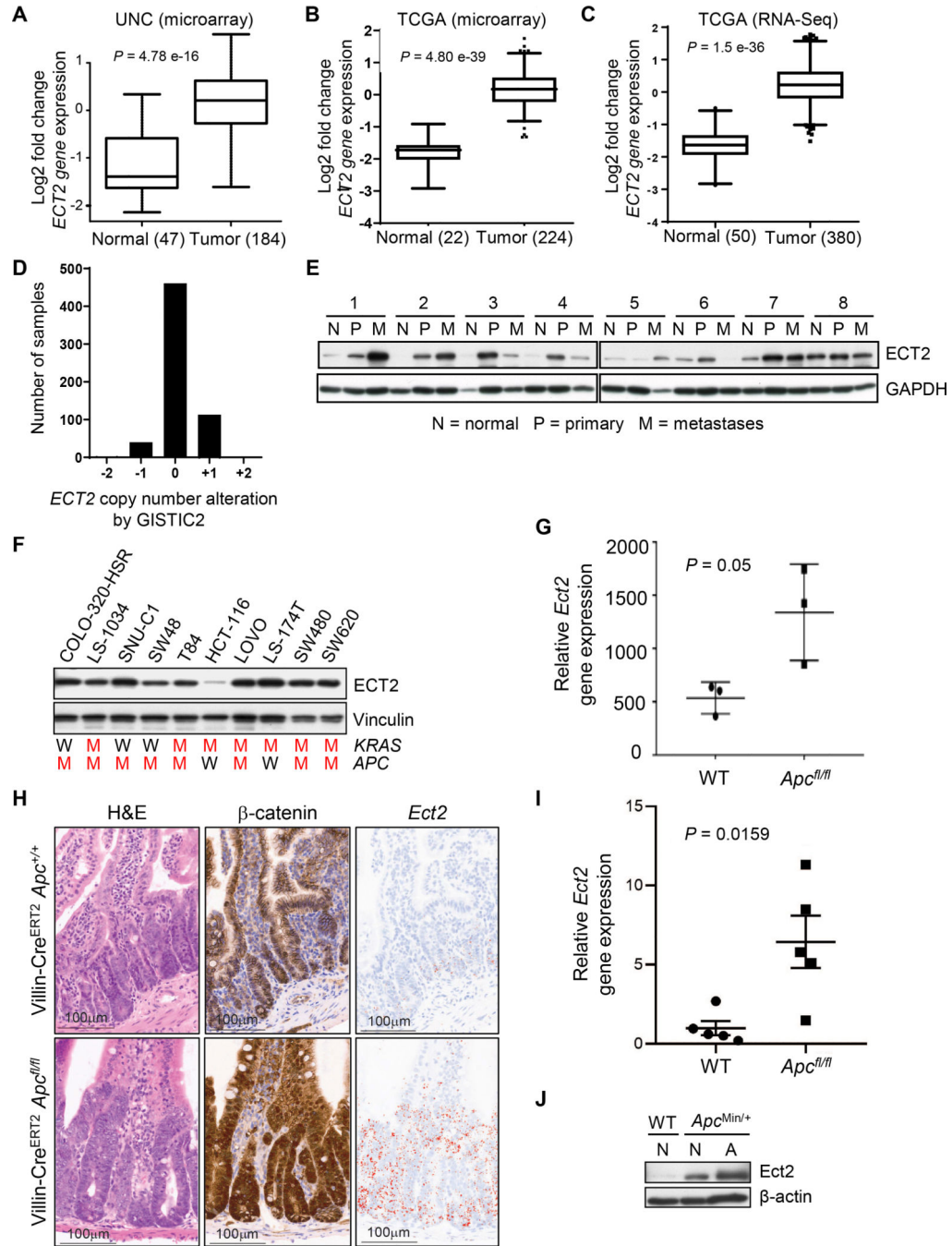
Statement of Significance

ECT2 overexpression and mislocalization support its role as a driver in colon cancer that is independent from its function in normal cell cytokinesis.
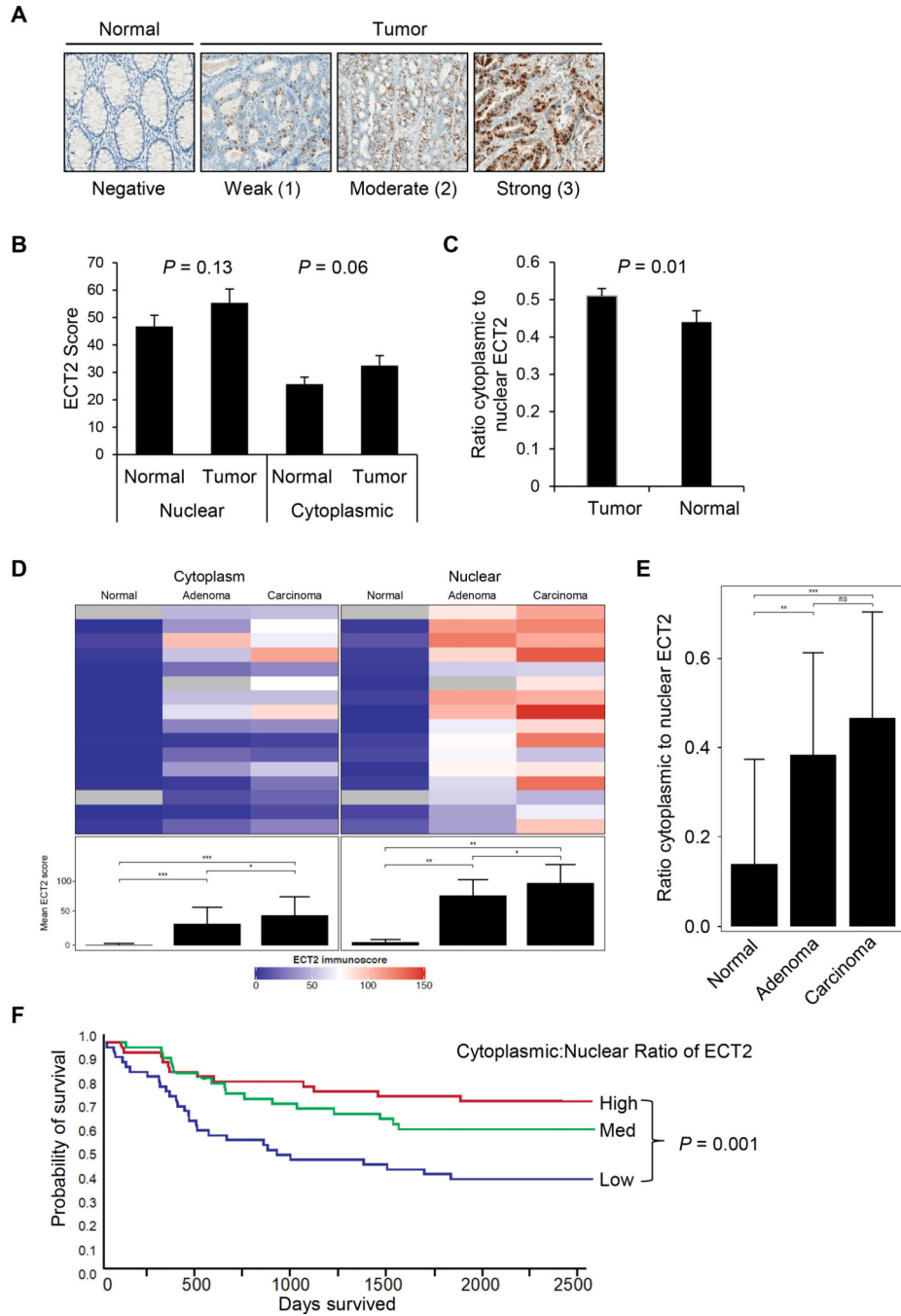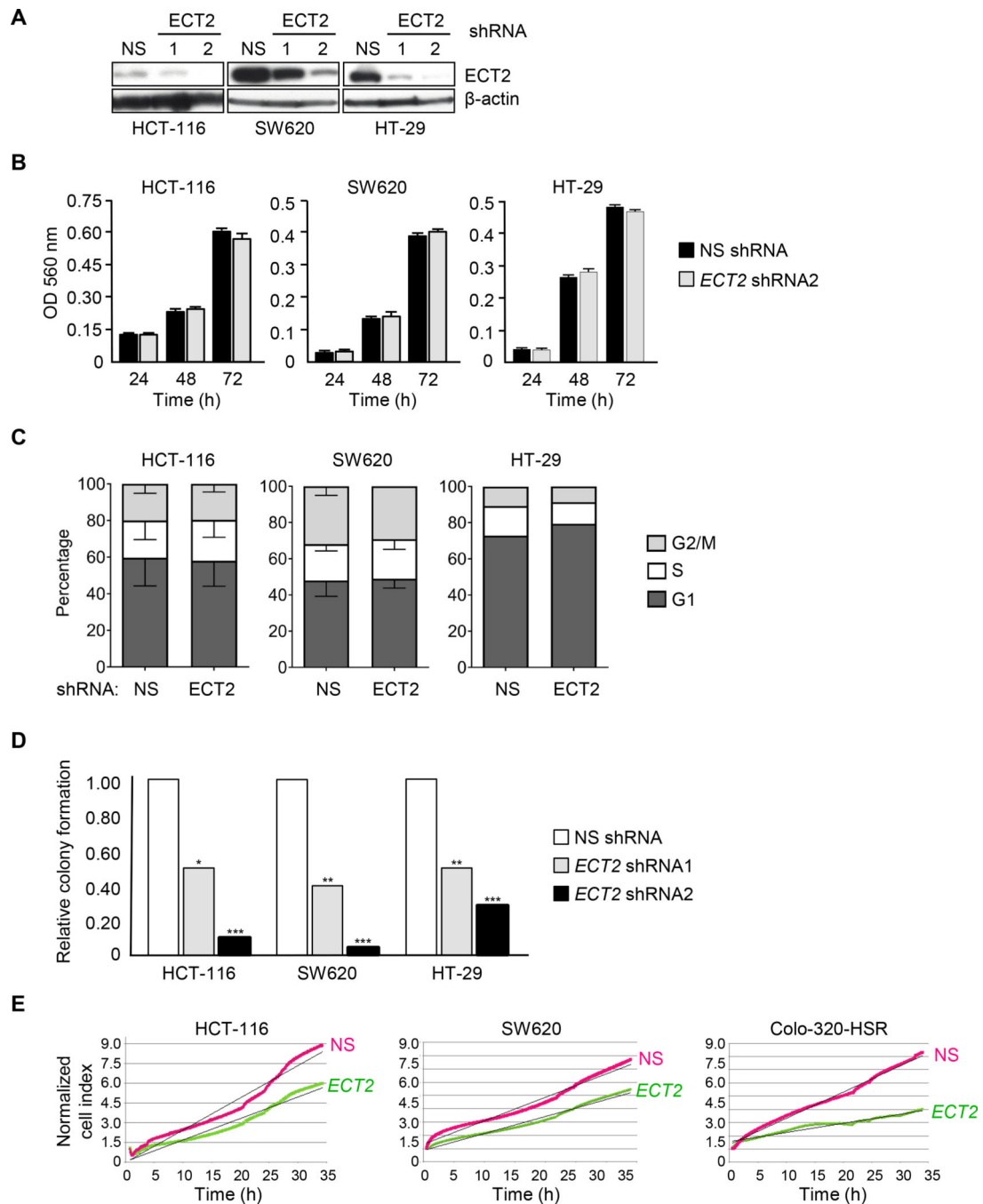
Figure 1.

Increased *ECT2* mRNA and protein expression in CRC. **A**, *ECT2* mRNA expression from a microarray of 47 normal colon samples compared to 184 tumor samples. **B**, *ECT2* mRNA levels in 224 CRC and 22 paired normal tissue samples from TCGA were analyzed on Agilent gene expression arrays. **C**, *ECT2* mRNA levels in 380 CRC and 50 paired normal tissue samples from TCGA were analyzed by RNA-Seq. **A-C**, Shown are median values in boxplot diagrams, *P*-values determined by a two-sided unpaired Student's *t* test. **D**, *ECT2* genomic copy number in 615 CRC samples from TCGA was determined by

GISTIC2. **E**, Immunoblot for ECT2 protein expression in normal (N), primary (P), and metastatic (M) tissues isolated from eight CRC patients. Immunoblot for GAPDH was done to verify equivalent loading of total protein. **F**, Immunoblot of cell lysates derived from the indicated human CRC cell lines, with immunoblot for vinculin to verify equivalent loading of total cellular protein (n = 1). *KRAS* and *APC* genotypes as indicated (W = wild-type, M = mutated, see Supplementary Table S1). **G**, RNA-seq analysis comparing whole tissue from the small intestine of wild-type (WT, Villin-Cre^{ERT2} *Apc$^{+/+}$*) and *Apc*-deficient (Villin-Cre^{ERT2} *Apc$^{fl/fl}$*) mice. Data are mean ± SEM, n = 3, *P*-value determined by two-tailed Mann-Whitney test. **H**, Representative images of hematoxylin and eosin (H&E) stained, anti-β-catenin immunohistochemically stained or *Ect2*-specific RNA-ISH (RNAscope) stained tissue specimens from the small intestine of wild-type (Villin-Cre^{ERT2} *Apc$^{+/+}$*) and Villin-Cre^{ERT2} *Apc$^{fl/fl}$* mice. Scale bar, 100 μm. **I**, Quantitation of the relative area of *Ect2*-positive epithelial staining from tissue specimens represented in **H** revealed increased *Ect2* gene expression in *Apc*-deficient intestines. Data are mean ± SEM, n = 5, *P*-value calculated by a two-tailed Mann-Whitney test. **J**, Representative immunoblot analyses for ECT2 protein expression in wild-type (WT) or *Apc$^{Min/+}$* mouse-derived normal (N) or adenoma (A) tissue. Representative data of two independent experiments, with quantitation provided in Supplementary Fig. S1D.

Figure 2.
Decreased ratio of cytoplasmic to nuclear ECT2 correlates with poorer overall survival. **A**, Representative IHC images for colorectal tumor and adjacent non-tumor colorectal tissues with weak, moderate, or strong intensity of total ECT2 staining (5x magnifications). **B**, Quantitation of the IHC analysis for ECT2 protein expression (ECT2 score) in cytoplasmic and nuclear compartments of CRC tumor and normal tissue. **C**, Increased C:N ratio of ECT2 expression in CRC tumor tissue, derived from scores in **B**. The ratio of ECT2 cytoplasmic score over ECT2 nuclear score was significantly higher in tumor compared to adjacent

normal tissues. **B-C**, Data are mean ± SEM, *P*-values determined by paired *t* test (29 TMAs, 146 patients). **D**, ECT2 score comparisons by cytoplasmic and nuclear locations determined in a smaller, independent IHC study. The heatmap visualizes (linear) IHC scores from cytoplasmic (left) and nuclear (right) staining in each of the 16 normal, adenoma or carcinoma tissues. Mean ECT2 scores derived from each column with all normal, adenoma or carcinoma tissues and significant tissue-dependent differences are shown below indicating significant differences in the nuclear compartment (normal vs. adenoma, *P* = 0.0002; adenoma vs. carcinoma, *P* = 0.0248; normal vs. carcinoma, *P* = 0.0001) and in the cytoplasmic compartment (normal vs. adenoma, *P* = 0.0016; adenoma vs. carcinoma, *P* = 0.0237; normal vs. carcinoma, *P* = 0.0011). Gray color indicates lack of respective tissue. **E**, Cytoplasmic to nuclear ratios (C:N) were derived from mean ECT2 scores (bar graphs) indicated in **D**. Increased C:N ratios of ECT2 were determined in adenoma and carcinoma compared to normal tissue (normal vs. adenoma *P* = 0.0028; adenoma vs. carcinoma, *P* = 0.32; normal vs. carcinoma, *P* = 0.0008). **D-E**, Data in bar graphs are mean ± SD, n = 16 patients, *P < 0.05, **P < 0.01, **P < 0.001; paired *t* test. **F**, Relationship between ECT2 C:N ratio based on the data in **B-C** and CRC patient survival, as shown by the Kaplan-Meier overall survival curve. *P*-value determined using log-rank test, see Table 1 for n.

Figure 3.

ECT2 is required for CRC cell line anchorage-independent growth and Matrigel invasion.

A, Depletion of ECT2 protein levels in CRC cell lines. Representative western blot of the indicated cell lines stably infected with lentivirus-based vectors expressing shRNA sequences targeting two different *ECT2* sequences or non-targeting (NS) shRNA as control.

B, The MTT viability assay was used to monitor proliferation of indicated CRC cell lines which were stably infected with NS shRNA or *ECT2* shRNA2. Data are mean ± SEM, n = 3.

C, Cell cycle analysis was done by DNA-content staining with propidium iodide (PI) of the

indicated CRC cell lines with either non-targeting (NS) shRNA or *ECT2* shRNA2. Data are mean ± SEM, n = 2 for HCT-116 and SW620, n = 1 for HT-29. **D**, Anchorage-independent growth (soft agar colony formation) normalized as a function of ECT2 expression in CRC cell lines. Data are normalized mean values, n = 3, $*P < 0.05$, $**P < 0.01$, $***P < 0.001$, unpaired t-test). **E**, Following stable ECT2 suppression via shRNA2, real-time analysis of Matrigel invasion (shown as normalized cell index) of indicated CRC cell lines was determined by the xCELLigence system; NS shRNA was used as control. Data shown are representative of two independent experiments.

A

B

C

Fabpl-Cre; *Apc*[2lox14/+]; *Kras*[LSL-G12D]; *Ect2*^{fl/fl}

19.9 weeks   23.6 weeks
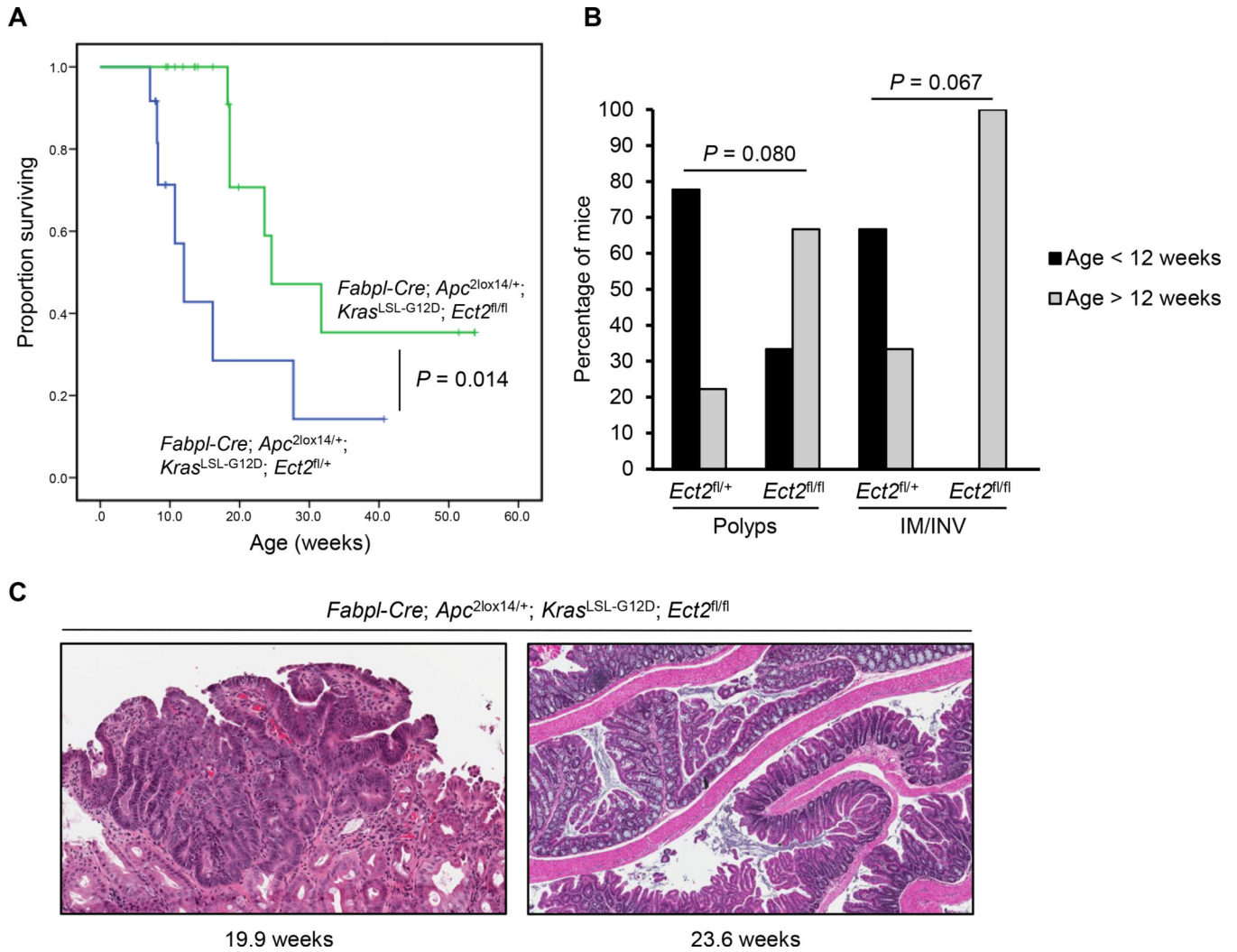
Figure 4.
Loss of Ect2 extends survival in a *Kras* and *Apc* driven CRC mouse model. **A**, Survival of *Fabpl-Cre*;Apc[2lox14/+]; *Kras*[LSL-G12D] mice with either heterozygous loss of *Ect2* (*Fabpl-Cre;Apc*[2lox14/+];*Kras*[LSL-G12D];*Ect2*^{fl/+}; n = 19) or homozygous loss of *Ect2* (*Fabpl-Cre;Apc*[2lox14/+];*Kras*[LSL-G12D];*Ect2*^{fl/fl}; n = 12), as shown by a Kaplan-Meier overall survival curve. *P*-value determined using log-rank test. **B**, Percentage of mice (genotype as indicated) forming polyps or intramucosal (IM) or invasive (INV) cancers at <12 week compared to >12 week of age. **C**, Representative H&E staining of intestines from *Fabpl-Cre;Apc*[2lox14/+];*Kras*[LSL-G12D];*Ect2*^{fl/fl} mice showing an intramucosal adenocarcinoma at 19.9 weeks and an invasive adenocarcinoma at 23.6 weeks.

A

B

C

D

E
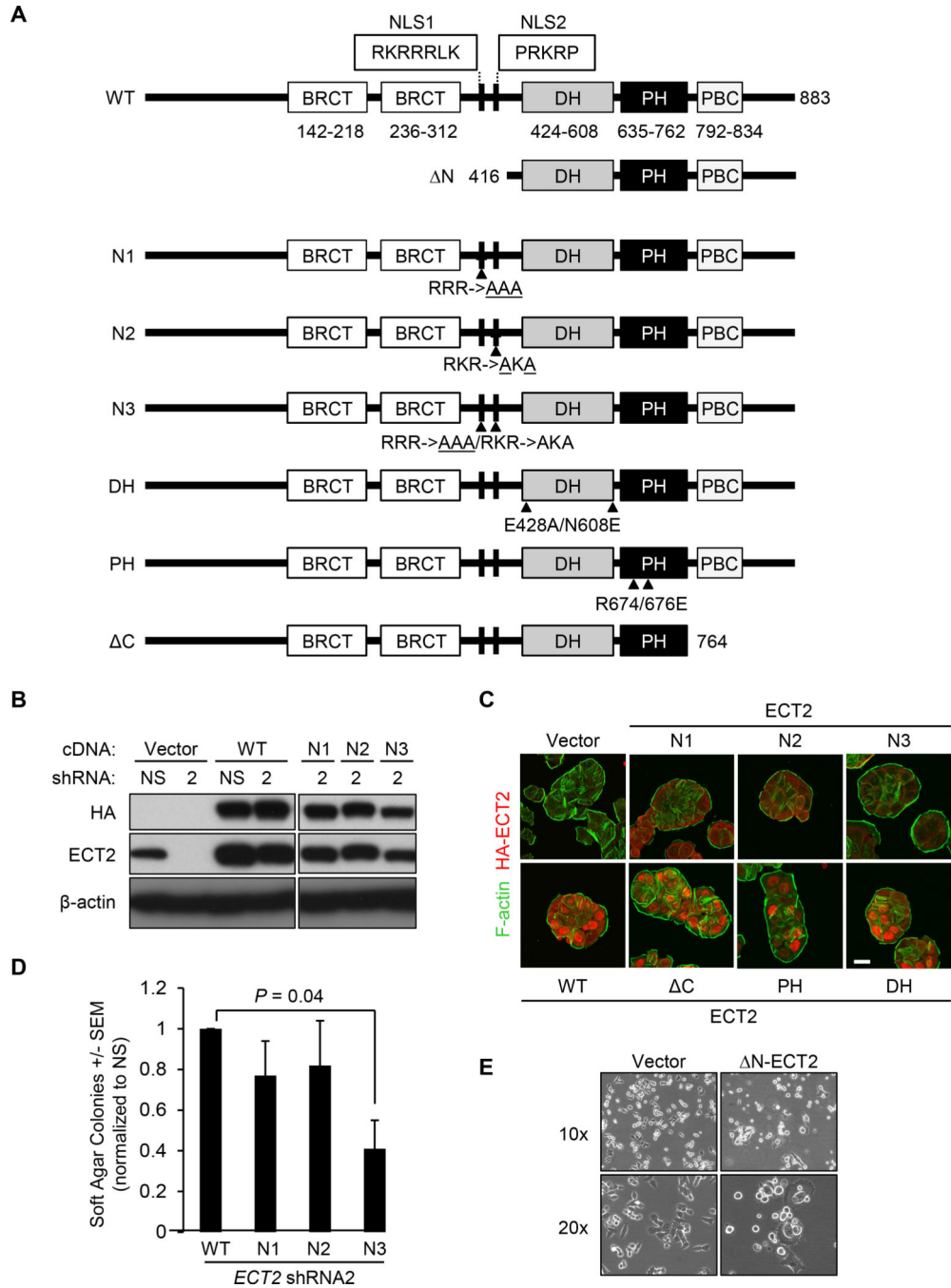
Figure 5.

Nuclear ECT2 is required to support anchorage-independent growth. **A**, Schematic overview of ECT2 mutants harboring missense or deletion mutations. Domain structure was determined in SMART. BRCT, BRCA1 carboxyl-terminus; DH, Dbl homology; PH, pleckstrin homology; PBC, polybasic cluster. **B**, Representative western blot of HT-29 cells with stable suppression of endogenous ECT2, via non-targeting (NS) shRNA or *ECT2* shRNA2 (2), and ectopic expression of the indicated HA epitope-tagged ECT2 mutants or empty vector (vector). **C**, Immunofluorescence microscopy analyses to determine

the subcellular localization of indicated HA-tagged ECT2 proteins ectopically expressed in HT-29 cells. F-actin was used as control to visualize cell size and morphology. Representative images are shown. Scale bar, 10 μm. Images representative for three independent experiments. **D**, Soft agar colony formation analysis of the ability of NLS ECT2 mutants to rescue shRNA-mediated stable suppression of endogenous ECT2 expression and reduced anchorage-independent growth in HT-29 cells. Data are mean ± SEM, n = 3, *P*-value determined by unpaired *t* test. **E**, Representative phase-contrast images to determine the cell morphology of HCT-116 cells transiently infected with the control empty vector or encoding constitutively activated N-ECT2 (top, 10x magnification; bottom, 20x magnification).
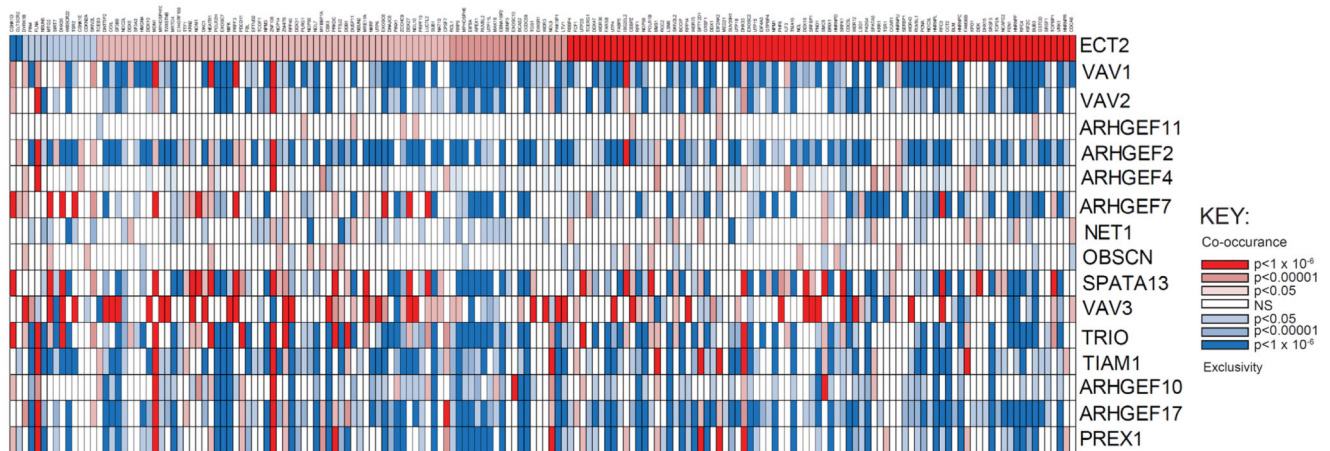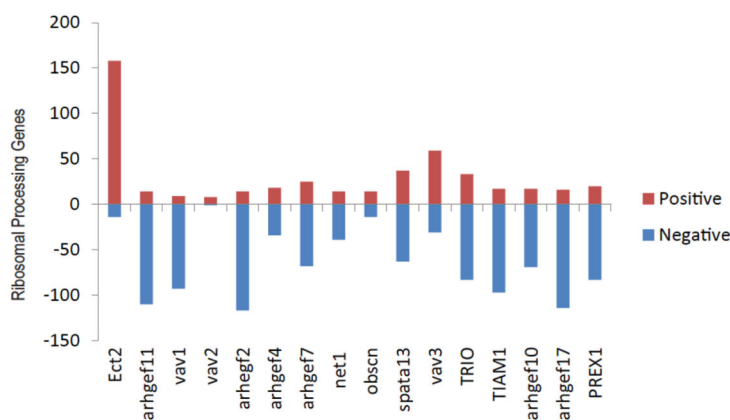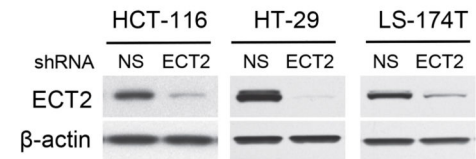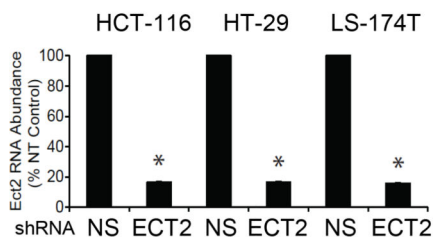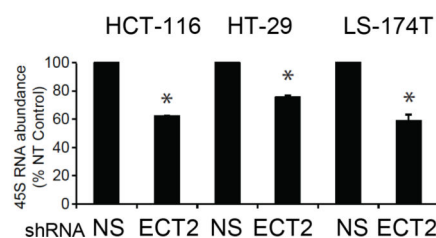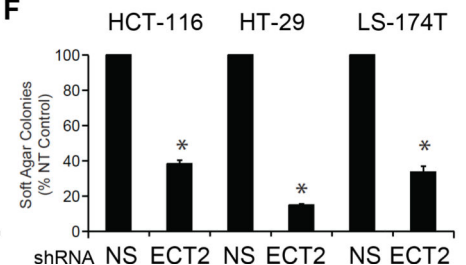
Figure 6.
ECT2 expression correlates with expression of ribosomal processing genes and regulates rRNA expression in CRC. **A**, Co-occurrence analysis of the TCGA CRC dataset (633 cases) for expression of 276 ribosomal processing genes and 16 RHOGEFs. Significant co-occurrences are shown in red and exclusivity in blue. *P*-values were derived using the Fisher's exact test. **B**, Bar graph depicting the number of ribosomal genes whose mean expression either positively (red) or negatively (blue) correlate with each of the indicated RHOGEFs. **C**, Stable control non-specific (NS) and shRNA suppression of ECT2 expression in the indicated CRC cell lines. Representative western blot analysis to monitor ECT2 suppression and equivalent loading of total cellular protein (β-actin). **D-E**, Consequences of ECT2 knockdown on ECT2 expression (**D**) or 45S rDNA abundance (**E**) was accessed by
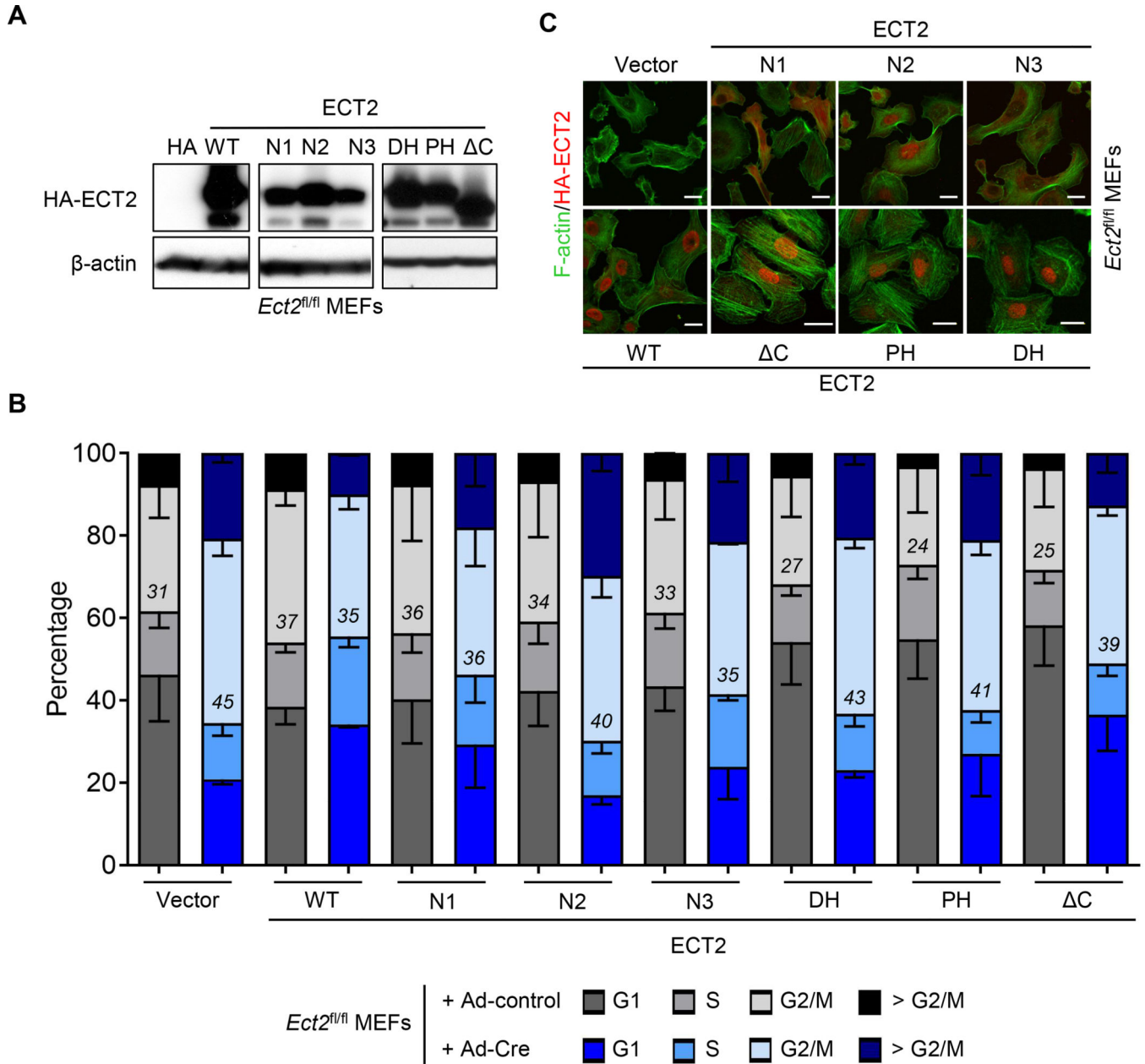
qPCR. **F**, Consequences of ECT2 knockdown on anchorage-independent growth in soft agar. Results in **D-F** represent mean ± SEM; n = 3. *$P < 0.05$ compared to NS.

Figure 7.
Nuclear localization is essential for ECT2 to support normal cell cytokinesis in mouse embryo fibroblasts. **A**, Representative western blot analysis of *Ect2$^{fl/fl}$* MEFs expressing indicated HA-tagged ECT2 mutants. **B**, Cell cycle analyses of MEFs exogenously expressing indicated HA-tagged ECT2 mutants and then treated with empty (Ad-control) or Cre adenovirus (Ad-Cre) to excise the endogenous *Ect2* allele. Data are mean ± SEM; n = 3. Determined percentage of cells in the G2/M phase is indicated. **C**, Immunofluorescence microscopy study to determine expression and subcellular localization of HA-tagged ECT2 mutants (red) ectopically expressed in *Ect2$^{fl/fl}$* MEFs. F-actin (green) was used as control

to visualize cell size and morphology. Images are representative for three independent experiments. Scale bar = 10 μm.

Table 1.

Associations between patient characteristics and tertiles of ECT2 scores

			ECT2		
Characteristic	**N**	**Low**	**Medium**	**High**	**P-value**
Age, mean (SE)	**139**	**66.1 (1.6)**	**67.0 (2.0)**	**65.1 2.1)**	**0.81**
Nuclear expression					
Gender, n (%)					
Male	77	24 (31)	26 (34)	27 (35)	0.54
Female	62	23 (37)	19 (31)	20 (32)	
Race, n (%)					
White	107	34 (32)	34 (32)	39 (36)	0.38
Black	29	11 (38)	10 (34)	8 (28)	
Stage, n (%)					
1+2	50	17 (34)	11 (22)	22 (44)	0.76
3+4	58	16 (28)	23 (40)	19 (33)	
Differentiation, n (%)					
Well	6	4 (66)	1 (17)	1 (17)	0.04
Mod	81	26 (32)	25 (31)	30 (37)	
Poor	18	3 (17)	6 (33)	9 (50)	
Location, n (%)					
Proximal	46	15 (33)	14 (30)	17 (37)	0.62
Distal	56	18 (32)	22 (39)	16 (29)	
Age, mean (SE)	139	67.8 (1.9)	67.0 (1.9)	63.5 (1.9)	0.25
Cytoplasmic to nuclear ratios					
Gender, n (%)					
Male	77	21 (27)	26 (34)	30 (39)	0.06
Female	62	26 (42)	19 (31)	17 (27)	
Race, n (%)					
White	107	39 (36)	34 (32)	34 (32)	0.29
Black	29	8 (28)	9 (31)	12 (41)	
Stage, n (%)					
1+2	50	12 (24)	16 (32)	22 (44)	0.77
3+4	58	14 (24)	21 (36)	23 (40)	
Differentiation, n (%)					
Well	3	0 (0)	2 (33)	4 (67)	0.48
Mod	57	22 (27)	27 (33)	32 (40)	
Poor	14	4 (22)	7 (39)	7 (39)	
Location, n (%)					
Proximal	46	19 (41)	15 (33)	12 (26)	0.07
Distal	56	15 (27)	18 (32)	23 (41)	

Abbreviations: n, number; SE, standard error